HHS Public Access

Author manuscript

Dev Dyn. Author manuscript; available in PMC 2017 April 01.

Published in final edited form as:

Dev Dyn. 2016 April ; 245(4): 497–507. doi:10.1002/dvdy.24389.

Syndactyly in a Novel *FRAS1*^{rdf} Mutant Results from Interruption of Signals for Interdigital Apoptosis

Elizabeth A. Hines[1], **Jamie M. Verheyden**[1], **Amber J. Lashua**[1], **Sarah C. Larson**[1], **Kelsey Branchfield**[1], **Eric T. Domyan**[1], **Juan Gao**[2], **Julie F. Harvey**[1], **John C. Herriges**[1], **Linghan Hu**[3], **David J. McCulley**[1], **Kurt Throckmorton**[1], **Shigetoshi Yokoyama**[1], **Akihiro Ikeda**[1], **Guoliang Xu**[2], and **Xin Sun**[1,*]

[1]Laboratory of Genetics, University of Wisconsin, Madison, WI 53706

[2]Institute of Biochemistry and Cell Biology, Shanghai Institute for Biological Sciences, Chinese Academy of Sciences, Shanghai, China 200031

[3]Zhiyuan College, Shanghai Jiao Tong University, Shanghai, China 200240

Abstract

Fras1 encodes an extracellular matrix protein that is critical for the establishment of the epidermal basement membrane during gestation. In humans, mutations in *FRAS1* cause Fraser Syndrome (FS), a pleiotropic condition with many clinical presentations such as limb, eye, kidney, and craniofacial deformations. Many of these defects are mimicked by loss of *Fras1* in mice, and are preceded by the formation of epidermal blisters *in utero*. In this study, we identified a novel ENU-derived *rounded foot* (*rdf*) mouse mutant with highly penetrant hindlimb soft-tissue syndactyly among other structural defects. Mapping and sequencing revealed that *rdf* is a novel loss-of-function nonsense allele of *Fras1* (*Fras1*^{rdf}). Focusing on the limb, we found that the *Fras1*^{rdf} syndactyly phenotype originates from loss of interdigital cell death (ICD). Despite normal expression of BMP ligands and their receptors, the BMP downstream target gene *Msx2,* which is also necessary and sufficient to promote ICD*,* was downregulated in the interdigital regions of *Fras1*^{rdf} hindlimb buds. The close correlation between limb bud epidermal blistering, decreased *Msx2* expression and reduced ICD suggest that epithelium detachment from the mesenchyme may create a physical gap that interrupts the transmission of BMP among other signals, resulting in soft tissue syndactyly.

Keywords

limb development; ENU screen; BMP signaling

Introduction

Fraser Syndrome (FS, OMIM 219000) is an autosomal recessive congenital disorder characterized by a spectrum of partially penetrant features including eye, limb, kidney, and

*Corresponding author: Xin Sun, Laboratory of Genetics, 425-G Henry Mall, University of Wisconsin, Madison, WI 53706, (608) 265-5405, xsun@wisc.edu.

craniofacial deformations. Epidemiological studies have estimated the incidence of FS to be 1 in 10,000 stillbirths and 1 in 500,000 live births (Martinez-Frias et al., 1998; Barisic et al., 2013). Multiple studies have determined the prevalence of various defects to be 75%–93% for cryptophthalmos, 54%–95% for syndactyly, 37%–84% for renal agenesis, and 7%–11% for craniofacial abnormalities (Thomas et al., 1986; Gattuso et al., 1987; Slavotinek and Tifft, 2002; van Haelst et al., 2007; Barisic et al., 2013). Past research using pedigree analyses have identified mutations in either of three distinct genes, *FRAS1, FRAS1-related extracellular matrix 2* (*FREM2*), and *GRIP1,* in FS patients (McGregor et al., 2003; Jadeja et al., 2005; Shafeghati et al., 2008; van Haelst et al., 2008; Vogel et al., 2012). Interestingly, analyses of various induced and spontaneous mutant mice exhibiting FS-like phenotypes have also identified *Fras1, Frem2, Grip1*, as well as *Frem1*, a homolog of *Frem2*, as loci for causative mutations (McGregor et al., 2003; Vrontou et al., 2003; Smyth et al., 2004; Takamiya et al., 2004; Jadeja et al., 2005; Miller et al., 2013). These mouse mutants have allowed for further study of the cellular and molecular mechanisms underlying the defects observed in FS.

Fras1 encodes a 4007 amino acid extra-cellular matrix (ECM) molecule expressed during embryonic development, which serves as an essential component of the basement membrane [reviewed in Short *et al* (Short et al., 2007)]. This large protein contains von Willebrand factor type C (VWFC) repeats, furin-like domains, chondroitin sulfate proteoglycan (neuron-glial antigen-2) repeats, and CALX-β cadherin-like domains. FRAS1 can associate with other matrix molecules including FREM1 and FREM2 to provide early adhesion during basement membrane formation (McGregor et al., 2003; Vrontou et al., 2003; Kiyozumi et al., 2006). *Fras1* is expressed by epithelial cells at sites of epithelial-mesenchyme interfaces including in the epidermis covering most of the body including the limb and eye, as well as in the kidney and lung (Vrontou et al., 2003; Chiotaki et al., 2007; Petrou et al., 2007; Pavlakis et al., 2008). Expression in these tissues begins as early as embryonic day 10.5 (E10.5) and in most tissues the expression level tapers off near birth (Short et al., 2007).

The requirement for *Fras1* in embryonic development of the skin, kidney, and palate has been investigated through the use of a variety of mutant alleles, including X-ray induced nonsense allele *blebbed* (*Fras1*^{bl}), ENU induced missense allele *blood-filled-blister* (*Fras1*^{bfb}), and a genetically engineered null allele (*Fras1*$^{-/-}$, deletion of exons 5 through 9) (McGregor et al., 2003; Vrontou et al., 2003; Miller et al., 2013). In the kidney, disruption of *Fras1* results in the downregulation of GDNF ligand expression and receptor tyrosine kinase (RTK) signaling, thereby preventing ureteric bud outgrowth into metanephric mesenchyme (Pitera et al., 2008; Pitera et al., 2012). In the skin, disruption of *Fras1* causes the epidermal cell layer to separate from the dermis, producing large blisters throughout the embryo (McGregor et al., 2003; Vrontou et al., 2003). These epidermal blisters persist into postnatal stages, often becoming hemorrhagic, affecting the growth and development of associated structures such as the eyelid (McGregor et al., 2003; Vrontou et al., 2003). Despite the variety of *Fras1* mutant alleles analyzed, the mechanism by which the epidermal blistering causes soft tissue syndactyly in the limb has not been elucidated.

In normal human and mouse limb development, the separation of individual digits requires precise spatial and temporal coordination of programmed cell death in the interdigital

mesenchyme. BMP signaling has been implicated as a key inducer of interdigital cell death (ICD) (Ganan et al., 1996; Yokouchi et al., 1996; Zou and Niswander, 1996; Macias et al., 1997; Merino et al., 1999; Pajni-Underwood et al., 2007). A variety of studies have demonstrated that loss of *Bmp2*, *Bmp4*, and *Bmp7* individually and in combination, or their receptor *Bmpr1a*, can result in syndactyly, indicating their essential role in ICD (Bandyopadhyay et al., 2006; Pajni-Underwood et al., 2007; Maatouk et al., 2009; Choi et al., 2012). For example, either epithelial or mesenchymal inactivation of Bmp ligand genes leads to syndactyly (Bandyopadhyay et al., 2006; Maatouk et al., 2009). These BMP ligands, acting through their receptors, induce the expression of *Msx1* and *Msx2,* transcription factor genes that are necessary and sufficient to trigger ICD (Ferrari et al., 1998; Brugger et al., 2004; Binato et al., 2006; Lallemand et al., 2009).

In an effort to identify novel mutations that are required for neonatal viability, we conducted an ENU-mutagenesis screen. One mutant identified in the screen was the *rounded foot (rdf)* mutant, which exhibited a variety of partially penetrant phenotypes including severe hindlimb soft tissue syndactyly, cleft palate, and kidney agenesis, phenocopying the plethora of phenotypes associated with FS. Using genetic mapping and candidate gene sequencing, we identified a novel nonsense mutation in the chondroitin sulfate proteoglycan (neuron-glial antigen-2) repeat domain of FRAS1. Possibly as a result of nonsense-mediated decay, *Fras1* mRNA level was significantly reduced in the *rdf* mutant. This result, and the similarity of phenotypes between the *rdf* mutant and the $Fras1^{-/-}$ knockout mutant suggest that $Fras1^{rdf}$ is a loss-of-function allele. Focusing on the mechanism underlying the hindlimb defects, our data suggest that blister-derived physical interruption of BMP signaling between the limb bud epithelium and mesenchyme may contribute to hindlimb syndactyly in these novel $Fras1^{rdf/rdf}$ mutants.

Results

Rounded foot (rdf) mutant identified in ENU mutagenesis screen

We carried out an ENU mutagenesis screen in mice to identify genes that are essential for embryonic development and neonatal viability. We mutagenized C57Bl/6J males (G0) and then outcrossed them to FVB females to generate G1 progeny. G1 males were mated to FVB females to generate G2 females. We then crossed each G1 male with its G2 female progeny and collected their G3 progeny via Caesarian (C)-section at E18.5 in order to observe their ability to thrive and to avoid cannibalization of unhealthy/stillborn mutants by the parents. G3 pups were then assessed for visual phenotypes. We found that one G1 male gave rise to G3 pups that exhibited hindlimb syndactyly, eye defects, cleft palate, and kidney loss (Figure 1).

To determine the penetrance of the various phenotypes, we analyzed 39 pups that displayed one or more defects (Table 1). Hindlimb syndactyly, the most penetrant feature (76.9%), was often accompanied by formation of a blood filled blister on either the dorsal, ventral, or both sides of the autopod (Figure 1A–C, E). Alcian blue and Alizarin red staining for cartilage and bone, respectively, revealed no skeletal element fusion, demonstrating that this phenotype results from soft tissue syndactyly (Figure 1E–G). While all autopod segments were present in the affected limbs, there was a deformation of the digits, ranging from slight

bends in the distal phalanges to complete inward curling of the phalanges and metacarpals (Figure 1F,G). Preaxial polydactyly was observed in the hindlimb in 10.3% of the mutants. All forelimbs observed at E18.5 were normal. Eye defects including blisters over the eyes and open eyelids were seen in 53.8% of the pups (Figure 1D). Cleft palate was found in 30.8% of pups (Figure 1M,N). Uni-lateral or bi-lateral kidney agenesis was observed in 28.2% of pups (Figure 1J–L). One mutant had a shortened tail with a blister on the distal tip (Figure 1I). No obvious left-right bias was observed in any of the tissue defects described above. Other organs, including the lung, were examined and no gross abnormalities were noted. Following their most conspicuous phenotype, the lack of separated digits and the rounded nature of their hindlimbs, we named these mutants *rounded foot* (*rdf*).

The viability of *rdf* mutants varied depending on the severity of their phenotypes, although no mutants survived until weaning age. All pups with cleft palate died within 2 hours of C-section. Pups with bi-lateral kidney agenesis were often stillborn, or died within two hours of C-section. Pups that survived until post-natal day 10 (P10) did not have kidney agenesis or cleft palate, however they often displayed eye defects, skin flaking, and limb deformation (Figure 1O). Interestingly, P10 *rdf* mutants were significantly smaller than controls and appeared to be developmentally delayed, suggesting that the *rdf* mutation impacts the ability to thrive.

Rounded foot (rdf) mutation is a nonsense allele of *Fras1*

Using PCR polymorphism mapping analysis, we narrowed the *rdf* containing region to a 13 megabase sequence on chromosome 5. This region contains 89 protein-coding genes. We searched the literature to determine if any of the genes contained in this region exhibited similar phenotypes when mutated. *Fras1* emerged as a top candidate gene since previously identified $Fras1^{bl/bl}$ and $Fras1^{-/-}$ mutants display phenotypes very similar to the *rdf* mutant (McGregor et al., 2003; Vrontou et al., 2003). We sequenced all 74 *Fras1* exons in one *rdf* mutant and found a nonsense mutation at base 4645 in exon 30, a sequence which encodes a portion of the chondroitin sulfate proteoglycan (neuron-glial antigen-2) repeat domain of FRAS1 (Figure 2A,C). The $Fras1^{rdf}$ point mutation was confirmed via sequencing in two additional mutants. All subsequent mutants were genotyped using PCR amplification and restriction enzyme digestion, since *HaeIII* digested the wild-type sequence whereas the *rdf* mutant sequence remained un-cut (Figure 2B). This cytosine to thymine mutation at base 4645 resulted in a change in the amino acid sequence of FRAS1 at amino acid 1263, changing a glutamine codon to a stop codon (Figure 2A,C). Thus, $Fras1^{rdf}$ is a nonsense allele. It occurs upstream of the $Fras1^{bl}$ nonsense mutation at amino acid 2200, also in the chondroitin sulfate (neuron-glial antigen-2) repeat domain, and the missense $Fras1^{bfb}$ mutation at amino acid 3588 near the C-terminus of FRAS1 (Figure 2C). To determine if the *Fras1* transcript level was affected in $Fras1^{rdf}$ mutants, we conducted qPCR analysis using cDNA from E13.5 control and mutant limb buds. *Fras1* transcript level in the mutant was significantly reduced to approximately a third of that in the control, possibly due to nonsense-mediated decay (Figure 2D). Given the location of the nonsense mutation, the decreased transcript level, and the $Fras1^{rdf}$ mutant phenocopying the $Fras1^{bl/bl}$, $Fras1^{bfb/bfb}$, and $Fras1^{-/-}$ phenotypes, the evidence suggests that the $Fras1^{rdf}$ mutation is a loss-of-function allele of *Fras1* (McGregor et al., 2003; Vrontou et al., 2003; Miller et al., 2013).

Fras1^{rdf} mutants exhibit decreased interdigital apoptosis in the developing hindlimb buds

Syndactyly often results from inadequate ICD during limb development. To assay for cell death in *Fras1*^{rdf} mutant limb buds, we utilized two independent methods: immunohistochemical staining for cleaved Caspase 3, an effecter of apoptosis, and vital dye labeling of apoptotic cells with Nile blue. As syndactyly was 76.9% penetrant in the analyzed *Fras1*^{rdf} mutants, we sampled a minimum of 8 mutant limb buds, including those with no apparent blistering and those with severe blistering. In general, by either cleaved Caspase 3 or Nile blue stainings, a similar range of staining patterns were observed. In comparing the interdigital regions of mutant to control limb buds at E13.5, the staining in the mutant limb buds ranged from markedly decreased (Figure 3A,B), to mildly decreased (Figure 3C,D), to normal (data not shown). Mutant limb buds with reduced ICD were observed at a frequency consistent with the penetrance of the E18.5 hindlimb syndactyly phenotype. Also, the extent of the ICD reduction correlated with the extent of blistering, as demonstrated by the strong ICD reduction in a limb bud with blister (Figure 3B) and the mild ICD reduction in a limb bud without blister (Figure 3D). Together, these results indicate that decreased ICD is closely associated with syndactyly observed in the *Fras1*^{rdf} mutants.

To better understand the spatial relationship of the blister to the AER and the mesenchyme, we sagittally sectioned E13.5 limb buds and examined the histology through hematoxylin and eosin staining (Figure 4A,B). Interestingly, the blisters in *Fras1*^{rdf} hindlimb buds were often observed on the dorsal and/or ventral sides of the autopod, and not over the AER. This suggests that tissue connection between the AER and underlying mesenchyme is preserved, whereas the connection between the dorsal and/or ventral epithelium and underlying mesenchyme may be interrupted. To determine if the AER or AER to mesenchyme signaling was affected in *Fras1*^{rdf} hindlimb buds, we assessed a key AER marker and signal, *Fgf8* expression, as well as the FGF downstream readouts *Spry2*, *Spry4* and *Dusp6* by *in situ* hybridization and qPCR. Previous studies show that an increase in AER-FGF expression can result in decreased ICD (Lu et al., 2006; Pajni-Underwood et al., 2007). We observed no significant difference in the expression of any of these genes, regardless of whether the mutant samples had blisters or not (Figure 4C–G and data not shown). These results suggest that blister formation does not affect AER-FGF to mesenchyme signaling.

Expression of BMP downstream effecters, but not upstream ligands and their principal receptor, is decreased in *Fras1*^{rdf} hindlimb buds

Previous studies have demonstrated that BMP signaling is essential for proper ICD and separation of the digits (Zou and Niswander, 1996; Bandyopadhyay et al., 2006; Pajni-Underwood et al., 2007; Maatouk et al., 2009; Choi et al., 2012). To elucidate if BMP ligand expression is changed in *Fras1*^{rdf} hindlimb buds, we performed qPCR for *Bmp2, Bmp4,* and *Bmp7* in E13.0 hindlimb buds. We found that ligand expression was unchanged in *Fras1*^{rdf} hindlimb buds compared to control (Figure 5A–C). To ascertain this normal expression does not result from compensatory spatial increases and decreases in the mutant compared to the controls, we performed RNA *in situ* hybridization for *Bmp2, Bmp4,* and *Bmp7*. We found no difference in the spatial expression patterns of these genes in the *Fras1*^{rdf} hindlimb buds compared to controls (Figure 5F–K). By qPCR, we also observed no difference in *Bmpr1a*

or *Bmpr2* receptor expression level in E13.0 *Fras1*^{rdf} hindlimbs compared to control (Figure 5D, E). These results together indicate the *Fras1*^{rdf} mutation does not affect the transcript levels of BMP ligands and their principal receptors.

BMP signaling activates the expression of *Msx2*, a transcription factor gene required for ICD and whose expression precedes apoptosis in the developing limb bud (Ferrari et al., 1998; Brugger et al., 2004; Lallemand et al., 2009). By RNA *in situ* hybridization, we found a consistent decrease in interdigital expression of *Msx2* in multiple *Fras1*^{rdf} hindlimb buds at E13.0 (Figure 6A,B). Hindlimb buds with apparent blisters always displayed decreased interdigital *Msx2* expression, and the frequency of limb buds with decreased expression was comparable to the penetrance of E18.5 syndactyly phenotype (Figure 6B and data not shown). Stained limb buds were sagittally sectioned to further compare regional patterns. *Msx2* expression at the digit tips in *Fras1*^{rdf} hindlimb buds did not appear different from control (Figure 6C,D). However, in the interdigital regions, *Msx2* staining was less intense, and occupied a smaller distal-to-proximal domain in *Fras1*^{rdf} limb buds compared to control (Figure 6E,F, horizontal lines). We found that the AER is a clear source of BMP ligands compared to the rest of the epithelium (Figure 6G,H), consistent with previous data (Maatouk et al., 2009). These observations raised the possibility that the gap generated by epithelium detachment may prevent efficient delivery of ligands from the epithelium to the underlying mesenchyme, thus affecting *Msx2* expression. This decrease in the interdigital *Msx2* expression preceded the decrease in interdigital cleaved Caspase 3 and Nile blue staining. These results, together with previous findings that *Msx2* is necessary and sufficient for ICD (Ferrari et al., 1998; Brugger et al., 2004; Binato et al., 2006; Lallemand et al., 2009), suggest that the decrease in *Msx2* expression in the *Fras1*^{rdf} hindlimb bud interdigital regions may contribute to the soft tissue syndactyly that develops in this mouse model of FS.

Discussion

In the present study we investigated *Fras1*^{rdf}, a novel loss-of-function allele of *Fras1* identified in our ENU mutagenesis screen. *Fras1*^{rdf} mutants exhibited a variety of phenotypes common in human Fraser Syndrome (FS) patients, including eye, kidney, and palate defects along with highly penetrant hindlimb syndactyly. Upon close examination, we found that the skeletal elements in the *Fras1*^{rdf} hindlimbs were not fused, but only mispositioned due to severe soft tissue syndactyly. Consistent with previous data that soft-tissue syndactyly often results from inadequate ICD during embryonic limb development, we found that ICD was decreased in the hindlimb buds of *Fras1*^{rdf} mutants. Furthermore, the frequency of ICD reduction correlated with the frequency of the epithelial blister on the autopod. To determine the possible molecular basis for this decrease of ICD, we focused on BMP signaling as it is the principle pathway implicated in this process. Interestingly, we found that while upstream ligand and receptor expression was unchanged in *Fras1*^{rdf} hindlimb buds, expression of the downstream effecter *Msx2* was decreased in the interdigital regions. We speculate that this decrease is likely a result of inefficient diffusion of the ligand from the epithelium to the mesenchyme due to blistering. As *Msx2* is necessary for proper ICD (Ferrari et al., 1998; Brugger et al., 2004; Lallemand et al., 2009), its decreased expression likely contributes to the syndactyly observed in *Fras1*^{rdf} mutants. While FGF signal from the AER to the limb bud mesenchyme does not seem to be affected, it remains

possible that blistering would hamper the delivery of additional signals other than BMP from the epithelium, thereby synergize with the effect of reduced BMP signaling on altering ICD. Furthermore, we speculate that the blister also loosens the normal mechanical constraint exerted by the ectoderm, resulting in transformation from the paddle-shaped autopod into a stump at later stages.

Fras1 is expressed in the epidermis throughout the body including the limb bud (Vrontou et al., 2003; Chiotaki et al., 2007; Petrou et al., 2007; Pavlakis et al., 2008). However, blisters were only found in selected tissues in *Fras1* mutants. For example, in late gestation (E18.5) $Fras1^{rdf}$ mutants, blisters were primarily observed in the hindlimbs. We speculate that the reason for the forelimb versus hindlimb differences could be molecular since multiple key patterning genes, such as *Tbx4* and *Tbx5* are differentially expressed between the forelimb and hindlimb buds (Rodriguez-Esteban et al., 1999). It is plausible that there are other basement membrane molecules that could compensate for the loss of *Fras1* specifically in the forelimb bud. Alternatively, the reason for the difference could be mechanical. It is plausible that the hindlimb buds, being localized near the umbilical cord and the tail, may be subjected to more external forces that initiate blistering than the forelimb buds. Additionally, developmental timing may play a role, as the hindlimb buds develop at a later time than the forelimb buds. The environment, for example the amniotic fluid pressure and content, may be different when the hindlimb buds are vulnerable to blistering compared to when the forelimb buds are. Within the hindlimb bud, the epithelium detachment was observed in the dorsal vs ventral surfaces but not the AER. This is likely because the AER is composed of specialized epithelial cells that are distinct from the flanking epithelium. For example, the AER, but not the flanking epithelium, expresses adhesion molecules such as Integrin alpha-6 and CD44 (Sherman et al., 1998; De Arcangelis et al., 1999). These molecules are known to play a role in the specialized behavior of AER cells. Furthermore, it has been shown that several other molecules similar to FRAS1, including FREM1, FREM2 and GRIP1 are often co-expressed with FRAS1 (Short et al., 2007). Subtle differences in the levels of these molecules in the AER versus flanking epithelium may affect their capability to compensate for the loss of FRAS1, contributing to why the flanking epithelium is more prone to detachment.

All the phenotypes in both the FS patients as well as in all FS mouse models, including $Fras1^{rdf}$, are partially penetrant. It was found that for the *Fras1* targeted allele $Fras1^{-/-}$, if carried in the C57BL/6 background, homozygous embryos die between E14.5 and E16.5. However, when the same mutation is moved to NMRI background, some of the homozygous embryos survive until adulthood (McGregor et al., 2003; Vrontou et al., 2003; Miller et al., 2013). These results suggest there are strong genetic modifiers in both the mouse as well as human genomic background to affect the penetrance of the FS phenotypes.

The finding that *Fras1* loss leads to syndactyly provides a clear example of the essential roles that structural proteins play in embryonic development. In a wide array of developing tissues, ECM components such as integrins and fibronectin are known to maintain structural integrity, facilitate cell movement, and assist in proper developmental signaling. For example, in the developing lung, genetic inactivation of *Integrin α8* results in lobe fusions, dilated distal airspaces, and defective sacculation (Benjamin et al., 2009). Inactivation of

Integrin β1 results in loss of epithelial integrity and failure to branch (Chen and Krasnow, 2012). In the developing retina, astrocyte expression of *FN* is essential to establish the ECM, which is required for sufficient VEGF binding and thus proper angiogenesis (Stenzel et al., 2011). Additionally, in the kidney, *Fras1* mutants exhibit defective expression of *Gdnf*, a growth factor ligand gene essential for proper ureteric budding (Pitera et al., 2008; Pitera et al., 2012). In contrast, in this study we show that within the limb bud, disruption of *Fras1* function did not affect BMP ligand or receptor expression. Rather, loss of *Fras1* led to epidermal blistering, which likely hinders BMP delivery to its target mesenchymal cells, resulting in lower *Msx2* expression, decreased ICD, and soft tissue syndactyly. This finding provides a novel mechanism of how disruption of *Fras1* function can impact tissue development.

Methods

ENU mutagenesis and screening

All mouse protocols were approved by University of Wisconsin-Madison Animal Care and Use Committee. Ten seven-week old C57BL/6J (Jax Stock # 000664) males were intra-peritoneally injected with N-ethyl-N-nitrosourea (ENU) (Sigma N3385) at a concentration of 100 mg/kg body weight once a week for three weeks. After a ten-week period of sterility and rest, males regained fertility and were mated with FVB (Jax Stock #001800) females to generate G1 males. Eighty G1 males were then crossed to FVB to generate G2 females. G1 males were crossed with their G2 female progeny to generate G3 embryos. E18.5 G3 pups were C-sectioned from time-mated females, counting noon on the day when the vaginal plug was found as embryonic day (E) 0.5. G3 pups were observed for two hours post C-section to assess viability. These G3 pups were then euthanized, and assessed for visual phenotypes both externally and internally. DNA was collected from G3 tails and purified using standard protocols.

Bone and Cartilage Staining

E18.5 G3 pups were isolated, skinned, eviscerated, and fixed in 95% EtOH for five days, with fresh 95% EtOH changed out every day. The fixed tissue was then stained with both Alcian blue (cartilage stain) and Alizarin red (bone stain) for three days using standard protocols. Tissues were cleared in 1% KOH and imaged.

PCR Polymorphism Mapping

Mapping primers for MIT microsatellite markers yielding disparate sized PCR products for C57BL/6J and FVB were identified using Mouse Genome Informatics (MGI) (www.informatics.jax.org/searches/polymorphism_form.shtml). Three sets of MIT primers spanning each chromosome were used for the initial screening of 8 *rdf* mutants. Regions of high C57BL/6J homozygosity were then more finely mapped with additional MIT markers spanning that region. The *rdf* containing region was sufficiently narrowed to the 47.29cM-53.2cM region on chromosome 5 by mapping 18 *rdf* mutants. A literature search was performed to investigate the 89 candidate genes in the regions and *Fras1* was selected for sequencing based on accordance with published mutant phenotypes (McGregor et al., 2003; Vrontou et al., 2003).

Sequencing and Restriction Digest Genotyping

Primers were designed to amplify each of the 74 exons in *Fras1.* Following PCR amplification of each exon from one *rdf* mutant, PCR products were gel purified using QIAquick Gel Extraction Kit (Qiagen) and manufacturer's instructions. Each exon was then sequenced in the forward and reverse direction using the BigDye® Terminator v3.1 Cycle Sequencing Kit (Life Technologies) following manufacturer's instructions. Sanger sequencing was conducted at the University of Wisconsin-Madison Biotechnology Center DNA Sequencing Facility. Sequences were analyzed using the open source A plasmid Editor (ApE) software (http://biologylabs.utah.edu/jorgensen/wayned/ape). The identified point mutation was confirmed by sequencing two additional *rdf* mutants. PCR-based genotyping was carried out using primers *Fras1* F: 5′-GTTCTCCACGTCAGCAAAGG-3′ and *Fras1* R: 5′-ACTGATAAATAGAGGCTGCAGG-3′ to amplify the mutation containing region and FastDigest *HaeIII* (Thermo-Fisher Scientific) to cleave the wild type product (Figure 2B).

Immunohistochemistry

E13.5 hindlimb buds were dissected in PBS, fixed in 4% paraformaldehyde overnight at 4°C, dehydrated to 100% MeOH, and stored at −20°C. Endogenous peroxidases were inactivated by washing the limbs in 6% H_2O_2 in 80% MeOH overnight at 4°C. Tissue was rehydrated and a standard whole mount immunohistochemistry protocol was carried out. Both the primary antibody, rabbit anti-cleaved Caspase 3 (Cell Signaling Technology), and the secondary antibody, goat anti-rabbit HRP (Sigma) were diluted 1:200 in 5% Normal Goat Serum using PBS with 0.1% Triton-X.

Nile Blue Staining

E13.5 embryos were dissected in PBS and incubated in DMEM solution (Life Technologies) containing 1.5% Nile Blue (Sigma N5632) at 37°C for one hour. Embryos were then rinsed in PBS and hindlimb buds were imaged.

Hematoxylin and Eosin Staining

E13.5 hindlimb buds were dissected in PBS, fixed in 4% paraformaldehyde overnight at 4°C, dehydrated to 70% EtOH, and embedded in paraffin. 7um sections were taken and stained with hematoxylin and eosin according to standard protocols.

Quantitative RT-PCR (qPCR)

E13.0 hindlimb buds for qPCR were dissected in DEPC PBS and homogenized in Trizol using the TissueLyser (Qiagen) and stored at −80°C. The reverse transcription reaction was carried out using the Superscript® III First Stand kit (Invitrogen) and manufacturer's instructions. qPCR was carried out using Power SYBR green (Applied Biosystems) and standard protocols. Primers used were *β-actin* F: 5′-CGGCCAGGTCATCACTATTGGCAAC-3′, *β-actin* R: 5′-GCCACAGGATTCCATACCCAAGAAG-3′; *Fras1* F: 5′-GGTATCACTGAACAATACTGCAC-3′, *Fras1* R: 5′-CACAAACGTCTCCAGTCCT-3′; *Bmp2* F: 5′-CTTCCATCACGAAGAAGCC-3′, *Bmp2* R: 5′-TGAGAAACTCGTCACTGGG-3′; *Bmp4* F: 5′-TGAGGAGTTTCCATCACGAA-3′, *Bmp4*

R: 5′-CACCTCATTCTCTGGGATGC-3′; *Bmp7* F: 5′-TCAACCTAGTGGAACATGAC-3′, *Bmp7* R: 5′-ATAGATCCTGAATTCGGCTG-3′; *Bmpr1a* F: 5′-CAGCGATGAATGTCTTCGAG-3′, *Bmpr1a* R: 5′-AAAGCTGTGAGTCTGGAGG-3′; *Fgf8* F: 5′-TAATTGCCAAGAGCAACGG-3′, *Fgf8* R: 5′-TAAAGGCCATGTACCAGCC-3′; *Spry2* F: 5′-GATTCAAGGGAGAGGGGTTG-3′, *Spry2* R: 5′-CTCCATCAGGTCTTGGCAGT-3′.

In situ hybridization (ISH)

E13.0 embryos were dissected in DEPC PBS, fixed in 4% paraformaldehyde overnight at 4°C, and then dehydrated to 100% MeOH. ISH was carried out using established protocols (Abler et al., 2011). Stained tissue for vibratome sectioning was fixed in 4% paraformaldehyde overnight at 4°C, washed in PBS, embedded in 4% low melting point agarose and vibratome sectioned at a thickness of 100um.

Acknowledgments

We would like to thank Dr. Kathryn Anderson and her laboratory members, especially Dr. Joaquim Grego Bessa for their guidance on setting up and conducting this ENU mutagenesis screen. We would like to thank Dr. Alex Shedlovsky and Dr. William F. Dove for their guidance on ENU mutagenesis, and Dr. Scott Weatherbee for his guidance on mapping and cloning of mutants. This work was supported by National Science Foundation Graduate Research Fellowship 2011101268 (to E.A.H), American Heart grant 0950041G, March of Dimes grant 6-FY10-339, and NHLBI RO1 HL119946, University of Wisconsin Genetics and SMPH funds for exploratory research, and the Romnes Faculty Fellowship from the University of Wisconsin Office of the Vice Chancellor for Research and Education with funding from the Wisconsin Alumni Research Foundation (to X.S.).

References

Abler LL, Mehta V, Keil KP, Joshi PS, Flucus CL, Hardin HA, Schmitz CT, Vezina CM. A high throughput in situ hybridization method to characterize mRNA expression patterns in the fetal mouse lower urogenital tract. J Vis Exp. 2011

Bandyopadhyay A, Tsuji K, Cox K, Harfe BD, Rosen V, Tabin CJ. Genetic analysis of the roles of BMP2, BMP4, and BMP7 in limb patterning and skeletogenesis. PLoS Genet. 2006; 2:e216. [PubMed: 17194222]

Barisic I, Odak L, Loane M, Garne E, Wellesley D, Calzolari E, Dolk H, Addor MC, Arriola L, Bergman J, Bianca S, Boyd PA, Draper ES, Gatt M, Haeusler M, Khoshnood B, Latos-Bielenska A, McDonnell B, Pierini A, Rankin J, Rissmann A, Queisser-Luft A, Verellen-Dumoulin C, Stone D, Tenconi R. Fraser syndrome: epidemiological study in a European population. Am J Med Genet A. 2013; 161A:1012–1018. [PubMed: 23532946]

Benjamin JT, Gaston DC, Halloran BA, Schnapp LM, Zent R, Prince LS. The role of integrin alpha8beta1 in fetal lung morphogenesis and injury. Dev Biol. 2009; 335:407–417. [PubMed: 19769957]

Binato R, Alvarez Martinez CE, Pizzatti L, Robert B, Abdelhay E. SMAD 8 binding to mice Msx1 basal promoter is required for transcriptional activation. Biochem J. 2006; 393:141–150. [PubMed: 16101586]

Brugger SM, Merrill AE, Torres-Vazquez J, Wu N, Ting MC, Cho JY, Dobias SL, Yi SE, Lyons K, Bell JR, Arora K, Warrior R, Maxson R. A phylogenetically conserved cis-regulatory module in the Msx2 promoter is sufficient for BMP-dependent transcription in murine and Drosophila embryos. Development. 2004; 131:5153–5165. [PubMed: 15459107]

Chen J, Krasnow MA. Integrin Beta 1 suppresses multilayering of a simple epithelium. PLoS One. 2012; 7:e52886. [PubMed: 23285215]

Chiotaki R, Petrou P, Giakoumaki E, Pavlakis E, Sitaru C, Chalepakis G. Spatiotemporal distribution of Fras1/Frem proteins during mouse embryonic development. Gene Expr Patterns. 2007; 7:381–388. [PubMed: 17251066]

Choi KS, Lee C, Maatouk DM, Harfe BD. Bmp2, Bmp4 and Bmp7 are co-required in the mouse AER for normal digit patterning but not limb outgrowth. PLoS One. 2012; 7:e37826. [PubMed: 22662233]

De Arcangelis A, Mark M, Kreidberg J, Sorokin L, Georges-Labouesse E. Synergistic activities of alpha3 and alpha6 integrins are required during apical ectodermal ridge formation and organogenesis in the mouse. Development. 1999; 126:3957–3968. [PubMed: 10433923]

Ferrari D, Lichtler AC, Pan ZZ, Dealy CN, Upholt WB, Kosher RA. Ectopic expression of Msx-2 in posterior limb bud mesoderm impairs limb morphogenesis while inducing BMP-4 expression, inhibiting cell proliferation, and promoting apoptosis. Dev Biol. 1998; 197:12–24. [PubMed: 9578615]

Ganan Y, Macias D, Duterque-Coquillaud M, Ros MA, Hurle JM. Role of TGF beta s and BMPs as signals controlling the position of the digits and the areas of interdigital cell death in the developing chick limb autopod. Development. 1996; 122:2349–2357. [PubMed: 8756280]

Gattuso J, Patton MA, Baraitser M. The clinical spectrum of the Fraser syndrome: report of three new cases and review. J Med Genet. 1987; 24:549–555. [PubMed: 3118036]

Jadeja S, Smyth I, Pitera JE, Taylor MS, van Haelst M, Bentley E, McGregor L, Hopkins J, Chalepakis G, Philip N, Perez Aytes A, Watt FM, Darling SM, Jackson I, Woolf AS, Scambler PJ. Identification of a new gene mutated in Fraser syndrome and mouse myelencephalic blebs. Nat Genet. 2005; 37:520–525. [PubMed: 15838507]

Kiyozumi D, Sugimoto N, Sekiguchi K. Breakdown of the reciprocal stabilization of QBRICK/Frem1, Fras1, and Frem2 at the basement membrane provokes Fraser syndrome-like defects. Proc Natl Acad Sci U S A. 2006; 103:11981–11986. [PubMed: 16880404]

Lallemand Y, Bensoussan V, Clement CS, Robert B. Msx genes are important apoptosis effectors downstream of the Shh/Gli3 pathway in the limb. Dev Biol. 2009; 331:189–198. [PubMed: 19422820]

Lu P, Minowada G, Martin GR. Increasing Fgf4 expression in the mouse limb bud causes polysyndactyly and rescues the skeletal defects that result from loss of Fgf8 function. Development. 2006; 133:33–42. [PubMed: 16308330]

Maatouk DM, Choi KS, Bouldin CM, Harfe BD. In the limb AER Bmp2 and Bmp4 are required for dorsal-ventral patterning and interdigital cell death but not limb outgrowth. Dev Biol. 2009; 327:516–523. [PubMed: 19210962]

Macias D, Ganan Y, Sampath TK, Piedra ME, Ros MA, Hurle JM. Role of BMP-2 and OP-1 (BMP-7) in programmed cell death and skeletogenesis during chick limb development. Development. 1997; 124:1109–1117. [PubMed: 9102298]

Martinez-Frias ML, Bermejo Sanchez E, Felix V, Calvo Celada R, Ayala Garces A, Hernandez Ramon F. Fraser syndrome: frequency in our environment and clinical-epidemiological aspects of a consecutive series of cases. An Esp Pediatr. 1998; 48:634–638. [PubMed: 9662850]

McGregor L, Makela V, Darling SM, Vrontou S, Chalepakis G, Roberts C, Smart N, Rutland P, Prescott N, Hopkins J, Bentley E, Shaw A, Roberts E, Mueller R, Jadeja S, Philip N, Nelson J, Francannet C, Perez-Aytes A, Megarbane A, Kerr B, Wainwright B, Woolf AS, Winter RM, Scambler PJ. Fraser syndrome and mouse blebbed phenotype caused by mutations in FRAS1/Fras1 encoding a putative extracellular matrix protein. Nat Genet. 2003; 34:203–208. [PubMed: 12766769]

Merino R, Rodriguez-Leon J, Macias D, Ganan Y, Economides AN, Hurle JM. The BMP antagonist Gremlin regulates outgrowth, chondrogenesis and programmed cell death in the developing limb. Development. 1999; 126:5515–5522. [PubMed: 10556075]

Miller KA, Gordon CT, Welfare MF, Caruana G, Bertram JF, Bateman JF, Farlie PG. bfb, a novel ENU-induced blebs mutant resulting from a missense mutation in Fras1. PLoS One. 2013; 8:e76342. [PubMed: 24143185]

Pajni-Underwood S, Wilson CP, Elder C, Mishina Y, Lewandoski M. BMP signals control limb bud interdigital programmed cell death by regulating FGF signaling. Development. 2007; 134:2359–2368. [PubMed: 17537800]

Pavlakis E, Makrygiannis AK, Chiotaki R, Chalepakis G. Differential localization profile of Fras1/Frem proteins in epithelial basement membranes of newborn and adult mice. Histochem Cell Biol. 2008; 130:785–793. [PubMed: 18563433]

Petrou P, Chiotaki R, Dalezios Y, Chalepakis G. Overlapping and divergent localization of Frem1 and Fras1 and its functional implications during mouse embryonic development. Exp Cell Res. 2007; 313:910–920. [PubMed: 17240369]

Pitera JE, Scambler PJ, Woolf AS. Fras1, a basement membrane-associated protein mutated in Fraser syndrome, mediates both the initiation of the mammalian kidney and the integrity of renal glomeruli. Hum Mol Genet. 2008; 17:3953–3964. [PubMed: 18787044]

Pitera JE, Woolf AS, Basson MA, Scambler PJ. Sprouty1 haploinsufficiency prevents renal agenesis in a model of Fraser syndrome. J Am Soc Nephrol. 2012; 23:1790–1796. [PubMed: 23064016]

Rodriguez-Esteban C, Tsukui T, Yonei S, Magallon J, Tamura K, Izpisua Belmonte JC. The T-box genes Tbx4 and Tbx5 regulate limb outgrowth and identity. Nature. 1999; 398:814–818. [PubMed: 10235264]

Shafeghati Y, Kniepert A, Vakili G, Zenker M. Fraser syndrome due to homozygosity for a splice site mutation of FREM2. Am J Med Genet A. 2008; 146A:529–531. [PubMed: 18203166]

Sherman L, Wainwright D, Ponta H, Herrlich P. A splice variant of CD44 expressed in the apical ectodermal ridge presents fibroblast growth factors to limb mesenchyme and is required for limb outgrowth. Genes Dev. 1998; 12:1058–1071. [PubMed: 9531542]

Short K, Wiradjaja F, Smyth I. Let's stick together: the role of the Fras1 and Frem proteins in epidermal adhesion. IUBMB Life. 2007; 59:427–435. [PubMed: 17654118]

Slavotinek AM, Tifft CJ. Fraser syndrome and cryptophthalmos: review of the diagnostic criteria and evidence for phenotypic modules in complex malformation syndromes. J Med Genet. 2002; 39:623–633. [PubMed: 12205104]

Smyth I, Du X, Taylor MS, Justice MJ, Beutler B, Jackson IJ. The extracellular matrix gene Frem1 is essential for the normal adhesion of the embryonic epidermis. Proc Natl Acad Sci U S A. 2004; 101:13560–13565. [PubMed: 15345741]

Stenzel D, Lundkvist A, Sauvaget D, Busse M, Graupera M, van der Flier A, Wijelath ES, Murray J, Sobel M, Costell M, Takahashi S, Fassler R, Yamaguchi Y, Gutmann DH, Hynes RO, Gerhardt H. Integrin-dependent and -independent functions of astrocytic fibronectin in retinal angiogenesis. Development. 2011; 138:4451–4463. [PubMed: 21880786]

Takamiya K, Kostourou V, Adams S, Jadeja S, Chalepakis G, Scambler PJ, Huganir RL, Adams RH. A direct functional link between the multi-PDZ domain protein GRIP1 and the Fraser syndrome protein Fras1. Nat Genet. 2004; 36:172–177. [PubMed: 14730302]

Thomas IT, Frias JL, Felix V, Sanchez de Leon L, Hernandez RA, Jones MC. Isolated and syndromic cryptophthalmos. Am J Med Genet. 1986; 25:85–98. [PubMed: 3099574]

van Haelst MM, Maiburg M, Baujat G, Jadeja S, Monti E, Bland E, Pearce K, Hennekam RC, Scambler PJ. Molecular study of 33 families with Fraser syndrome new data and mutation review. Am J Med Genet A. 2008; 146A:2252–2257. [PubMed: 18671281]

van Haelst MM, Scambler PJ, Hennekam RC. Fraser syndrome: a clinical study of 59 cases and evaluation of diagnostic criteria. Am J Med Genet A. 2007; 143A:3194–3203. [PubMed: 18000968]

Vogel MJ, van Zon P, Brueton L, Gijzen M, van Tuil MC, Cox P, Schanze D, Kariminejad A, Ghaderi-Sohi S, Blair E, Zenker M, Scambler PJ, Ploos van Amstel HK, van Haelst MM. Mutations in GRIP1 cause Fraser syndrome. J Med Genet. 2012; 49:303–306. [PubMed: 22510445]

Vrontou S, Petrou P, Meyer BI, Galanopoulos VK, Imai K, Yanagi M, Chowdhury K, Scambler PJ, Chalepakis G. Fras1 deficiency results in cryptophthalmos, renal agenesis and blebbed phenotype in mice. Nat Genet. 2003; 34:209–214. [PubMed: 12766770]

Yokouchi Y, Sakiyama J, Kameda T, Iba H, Suzuki A, Ueno N, Kuroiwa A. BMP-2/-4 mediate programmed cell death in chicken limb buds. Development. 1996; 122:3725–3734. [PubMed: 9012494]

Zou H, Niswander L. Requirement for BMP signaling in interdigital apoptosis and scale formation. Science. 1996; 272:738–741. [PubMed: 8614838]

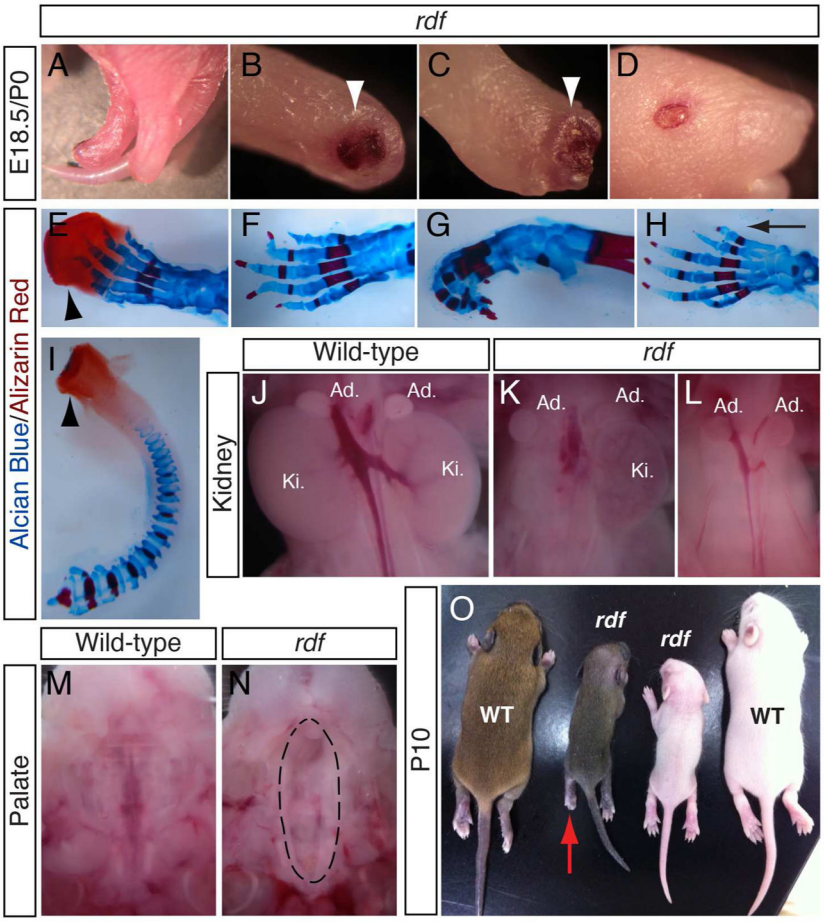

Figure 1. Rounded foot(*rdf*) mutants exhibit a variety of phenotypes

(A–C) Lateral view of the hindlimbs and tail (A) and magnified views of *rdf* mutant hindlimbs (B,C) following C-section at E18.5 showing the rounded limbs. White arrowheads indicate the epidermal blister. (D) Lateral view of *rdf* mutant head showing open eye at E18.5. (E–I) Alcian Blue and Alizarin Red staining for cartilage and bone respectively in *rdf* mutant hindlimbs (E–H) and tail (I) at E18.5. Arrowheads indicate epidermal blisters. Arrow indicates preaxial polydactyly. (J–L) Views of the kidneys and adrenal glands at E18.5 when *rdf* mutants exhibit either uni-lateral kidney agenesis (K) and bi-lateral kidney agenesis (L). (M,N) View of the upper palate showing cleft palate in *rdf* mutants at E18.5 (dashed outline). (O) P10 control and *rdf* pups showing that mutants are smaller in size. Red arrow indicates the affected hindlimb in the *rdf* mutant. Abbreviations: Ad., adrenal gland; Ki., kidney.

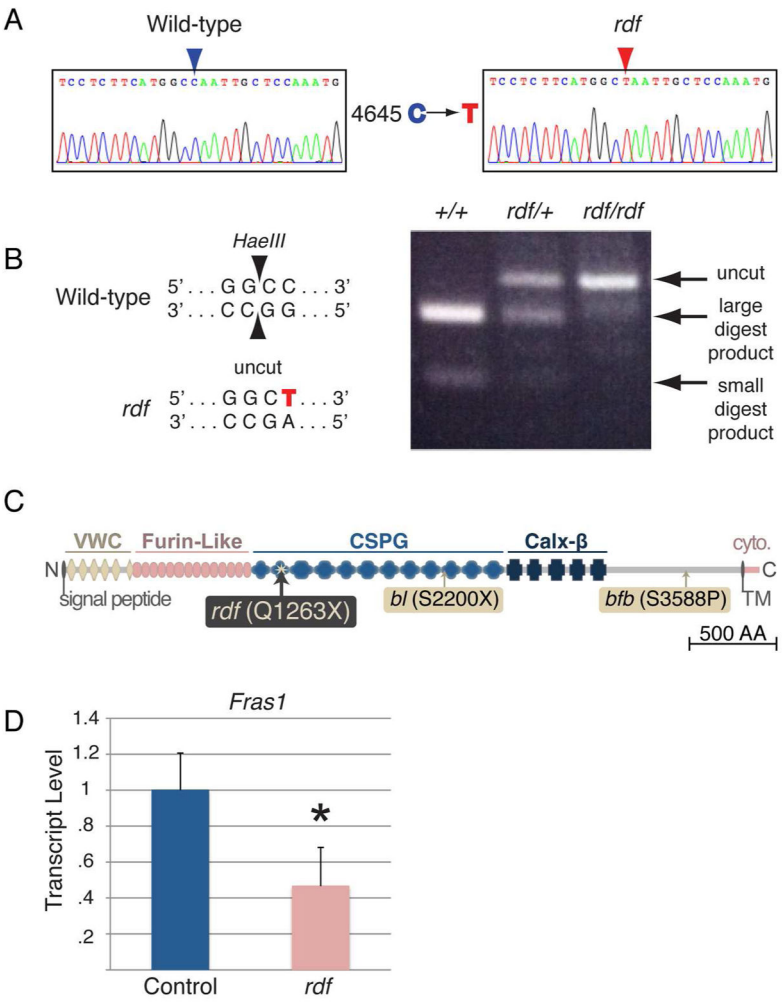

Figure 2. *rdf* mutants contain a nonsense mutation in *Fras1*

(A) DNA sequence of *Fras1* at position 4632–4659 in wild-type (left) and *rdf* (right). Blue arrowhead indicates the cytosine at base 4645 in wild-type and red arrowhead indicates the thymine at base 4645 in the *rdf* mutant. (B) *HaeIII* digested the control sequence whereas the *rdf* mutation prevented the digest. The gel image shows the restriction fragment length differences resulting from PCR amplification and *HaeIII* digestion. *+/+* indicates wild-type DNA, *rdf/+* indicates heterozygote DNA, *rdf/rdf* indicates homozygous DNA. (C) Scaled diagram of FRAS1 protein structure with the location of the *rdf* allele as well as other known point mutant alleles, *bl* and *bfb*, indicated. The genetically engineered null allele contains a lacZ/neo cassette inserted into exon 6 in the VWC domain, resulting in the absence of FRAS1 protein (Vrontou et al., 2003). N indicates the N-terminus, VWC indicates the von Willebrand factor type C repeats, CSPG indicates the chondroitin sulfate proteoglycan (neuron-glial antigen-2) repeats, TM indicates the transmembrane domain, cyto indicates the cytosolic portion, and C indicates the C-terminus. (D) By qRT, *Fras1* transcript level in the *rdf* E13.5 hindlimb buds is reduced when normalized to the control (normalized control= 1 ± 0.206, mutant= 0.465 ± 0.216, p=0.002, n=5 for each genotype). * indicates $p < 0.005$.

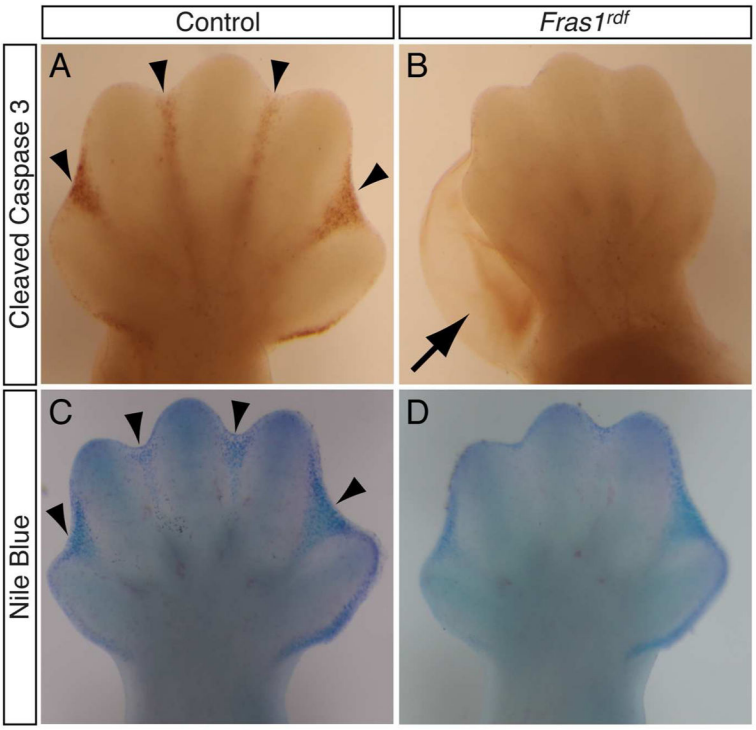

Figure 3. Interdigital cell death (ICD) is decreased in *Fras1*^{rdf} mutants

E13.5 hindlimb buds were analyzed by immunohistochemical staining for cleaved Caspase 3 (A,B), or vital dye Nile blue staining (C,D). Black arrowheads in A and C indicate regions of ICD in control tissue that are absent or reduced in mutant limbs. Black arrow in B indicates a severe blister in a *Fras1*^{rdf} hindlimb bud with a strong phenotype.

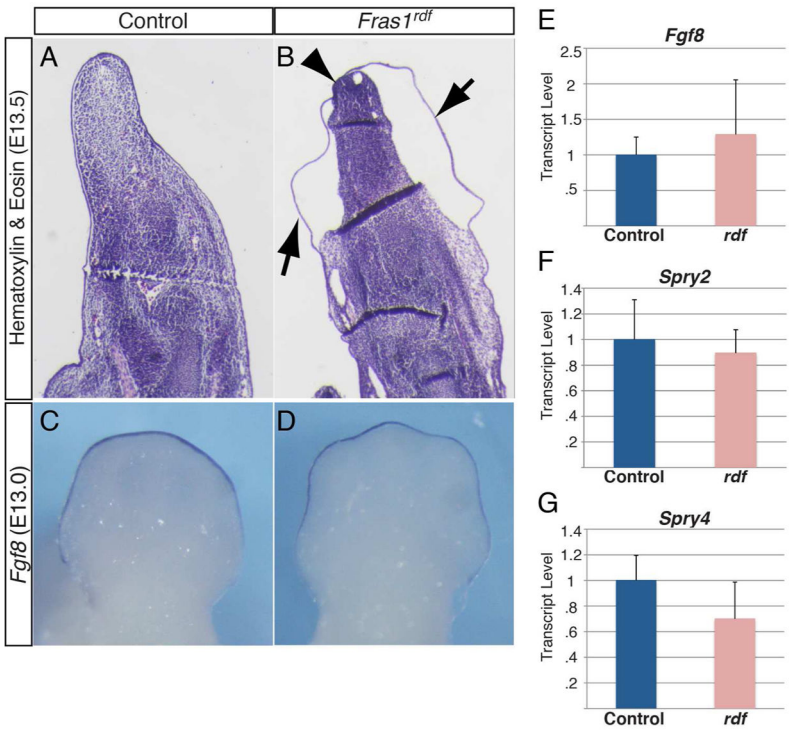

Figure 4. AER-*Fgf8* ligand and readout expression is unchanged in *Fras1*^{rdf} hindlimb buds

(A,B) H&E histological stain of E13.5 sagittal sections of hindlimb buds. Arrows indicate blisters on dorsal and ventral sides and arrowhead indicates the AER. (C,D) RNA *in situ* hybridization for *Fgf8* in E13.0 hindlimb buds. (E–G) Transcript levels of *Fgf8* and FGF activity readout genes *Spry2* and *Spry4* are not significantly altered in E13.0 *Fras1*^{rdf} mutant versus control hindlimb buds by qRT (for *Fgf8:* normalized control= 1 ± 0.243, mutant= 1.287 ± 0.746, p=0.451; for *Spry2:* normalized control= 1 ± 0.310, mutant= 0.894 ± 0.182, p=0.534; for *Spry4:* normalized control= 1 ± 0.195, mutant= 0.650 ± 0.288, p=0.095; n=5 for each genotype).

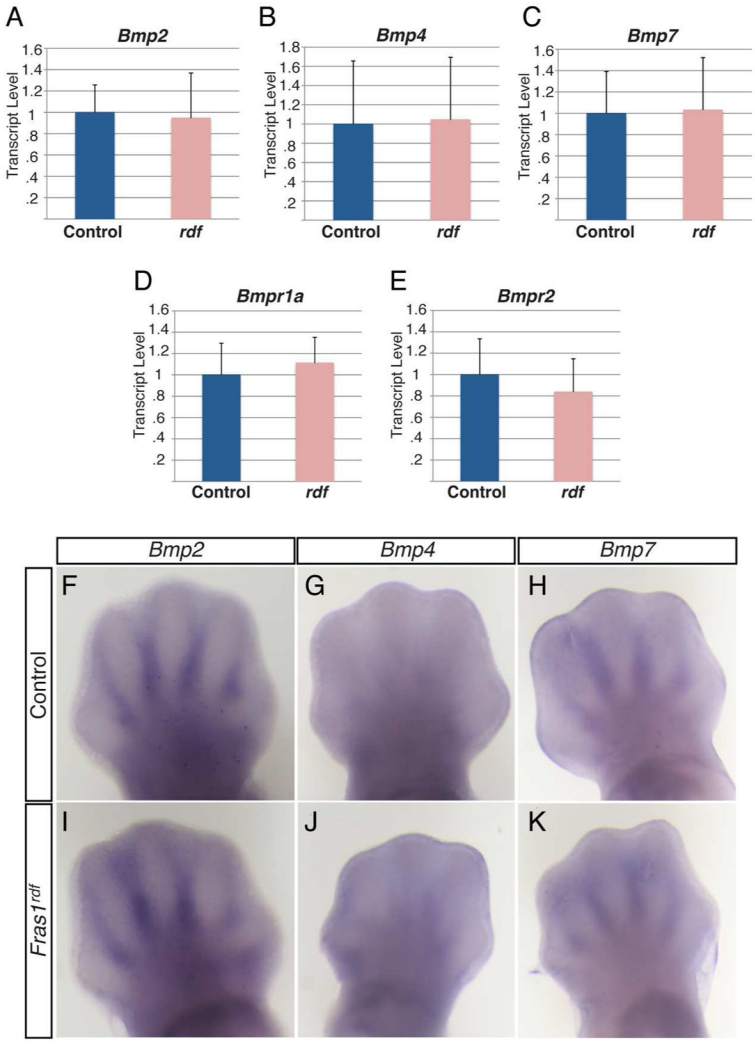

Figure 5. BMP ligand and receptor expression is unchanged in *Fras1*^{rdf} hindlimb buds

(A–E) Transcript levels of *Bmp2*, *Bmp4*, *Bmp7*, *Bmpr1a* and *Bmpr2* are not significantly altered in E13.0 *Fras1*^{rdf} mutant versus control hindlimb buds by qRT (for *Bmp2*, for *Bmp2*, control = 1 ± 0.257, mutant = 0.946 ± 0.422, p=0.815; for *Bmp4*, control = 1 ± 0.656, mutant = 1.045 ± 0.649, p=0.91; for *Bmp7*, control = 1 ± 0.390, mutant = 1.031 ± 0.490, p=0.915; for *Bmpr1a*, control = 1 ± 0.297, mutant = 1.111 ± 0.241, p=0.737; for *Bmpr2*, control = 1 ± 0.335, mutant = 0.837 ± 0.310, p=0.448; n=5 for each genotype). (F–K) RNA *in situ* hybridization for *Bmp2* (F,I), *Bmp4* (G,J), and *Bmp7* (H,K) in E13.0 control (F–H) and *Fras1*^{rdf} hindlimb buds (I–K) showing no change in expression patterns.

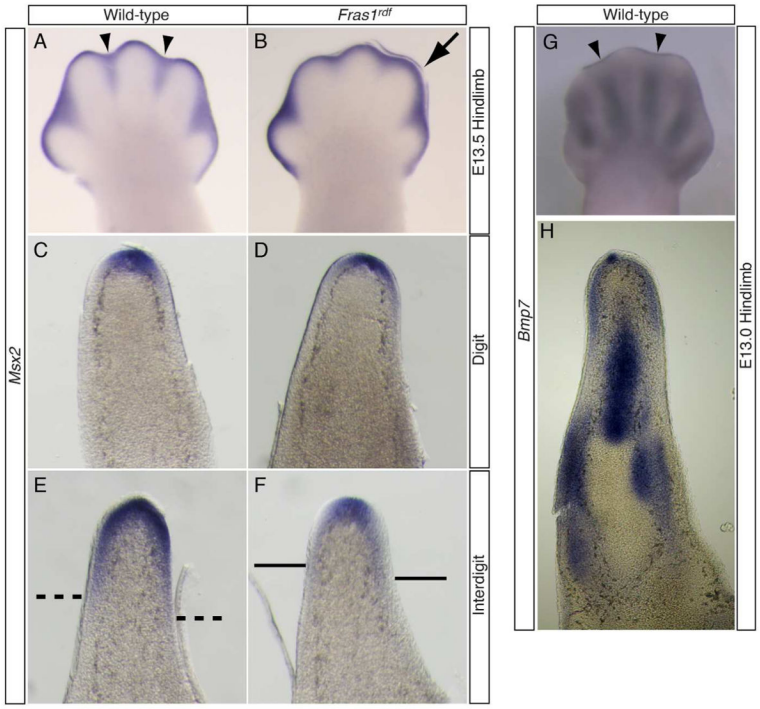

Figure 6. *Msx2* expression is decreased in the interdigital regions of *Fras1*^{rdf} hindlimb buds

(A–F) RNA *in situ* hybridization for *Msx2* in E13.0 hindlimb buds. (C–F) Sagittal 100um vibratome sections of above *Msx2* stained hindlimb bud digit region (C,D) and interdigit region (E,F). Dashed lines indicate the proximal boundaries of *Msx2* staining domain in the control interdigit region. Solid lines indicate the proximal boundaries of *Msx2* staining domain in the *Fras1*^{rdf} interdigit region. (G) RNA *in situ* hybridization for *Bmp7* in E13.0 wild-type hindlimb buds. Arrowheads indicate interdigit regions. (H) Sagittal 100um vibratome sections of above *Bmp7* stained hindlimb bud interdigit region show staining primarily in the AER and several regions of the mesenchyme.

Table 1

Penetrance of phenotypes in *rdf* mutants at E18.5

Phenotype	Affected/Total Mutants	Penetrance
Hindlimb Syndactyly	30/39	76.9%
Open Eyelids	21/39	53.8%
Cleft Palate	12/39	30.8%
Kidney Agenesis	11/39	28.2%
Polydactyly	4/39	10.3%
Tail Blister	1/39	2.6%

* Both unilateral or bilateral phenotypes were considered.